Poly(L-glutamic acid)-cisplatin nanoformulations with detachable PEGylation for prolonged circulation half-life and enhanced cell internalization

Zhongyu Jiang [a,b], Xiangru Feng [a], Haoyang Zou [a], Weiguo Xu [a,*], Xiuli Zhuang [a,b,**]

[a] *Key Laboratory of Polymer Ecomaterials, Changchun Institute of Applied Chemistry, Chinese Academy of Sciences, 5625 Renmin Street, Changchun, 130022, P. R. China*
[b] *School of Applied Chemistry and Engineering, University of Science and Technology of China, 96 Jinzhai Road, Hefei, 230026, P. R. China*

ARTICLE INFO

ABSTRACT

PEGylation has been widely applied to prolong the circulation times of nanomedicines *via* the steric shielding effect, which consequently improves the intratumoral accumulation. However, cell uptake of PEGylated nanoformulations is always blocked by the steric repulsion of PEG, which limits their therapeutic effect. To this end, we designed and prepared two kinds of poly(L-glutamic acid)-cisplatin (PLG-CDDP) nanoformulations with detachable PEG, which is responsive to specific tumor tissue microenvironments for prolonged circulation time and enhanced cell internalization. The extracellular pH (pH_e)-responsive cleavage 2-propionic-3-methylmaleic anhydride (CDM)-derived amide bond and matrix metalloproteinases-2/9 (MMP-2/9)-sensitive degradable peptide PLGLAG were utilized to link PLG and PEG, yielding pH_e-responsive PEG-pH_e-PLG and MMP-sensitive PEG-*MMP*-PLG. The corresponding smart nanoformulations PEG-pH_e-PLG-Pt and PEG-*MMP*-PLG-Pt were then prepared by the complexation of polypeptides and cisplatin (CDDP). The circulation half-lives of PEG-pH_e-PLG-Pt and PEG-*MMP*-PLG-Pt were about 4.6 and 4.2 times higher than that of the control PLG-Pt, respectively. Upon reaching tumor tissue, PEG on the surface of nanomedicines was detached as triggered by pH_e or MMP, which increased intratumoral CDDP retention, enhanced cell uptake, and improved antitumor efficacy toward a fatal high-grade serous ovarian cancer (HGSOC) mouse model, indicating the promising prospects for clinical application of detachable PEGylated nanoformulations.

1. Introduction

The technique of binding poly(ethylene glycol) (PEG) to a given platform is known as "PEGylation", which is a well-established strategy to develop drug delivery systems for systematic administration [1,2]. PEGylation generates a hydrated cloud with a large excluded volume around nanoparticles to sterically block the interaction between the nanoparticles and components in the blood [3]. Meanwhile, the flexibility of PEG provides considerable conformational freedom, which was thermodynamically unfavorable to the penetration of foreign matters into PEG corona [4]. Therefore, PEGylation leads to reduced protein adsorption and clearance *in vivo* and endows the nanoparticles with prolonged blood circulation time and increased drug accumulation in the target site by the enhanced permeability and retention (EPR) effect [4–6].

However, PEGylation always causes limited nanoparticle internalization by cancer cells because of the steric repulsion and water-cushion effect between PEG chains and cell membrane [7], which inevitably reduces the bioavailability of nanomedicines [8]. To overcome this "PEG dilemma", various tumor microenvironment-responsive dePEGylation strategies have been extensively investigated, including physical and chemical stimuli-responsive dePEGylation, aiming to trigger the extracellular shedding of PEG when nanoparticles enter the tumor tissue [1, 9]. Specifically, physical stimuli-responsive dePEGylation is mainly

based on the non-covalent adsorption of PEG to the nanoparticle surface [10], and chemical stimuli-responsive dePEGylation is based on the covalent bond with stimuli-responsive cleavage to bridge the PEG and nanoparticles, such as benzoic-imine bond, β-aminoacrylate bond, and peptide GGGVPLSLYSGGGG [11]. Upon reaching the tumor tissue, physical or chemical dePEGylation is triggered by specific tumor microenvironments, *e.g.*, low pH, redox potential, overexpressed enzymes, so that the nanoparticles without PEG shell could enter and deliver the drug to cancer cells more effectively. With this dePEGylation strategy, nanoparticles can benefit from both long circulation time and efficient drug delivery to target cancer cells [1].

Compared with other polymer nanoparticles, the polypeptide nanoparticles have gained wide attention in the field of biomaterials due to their unique properties, especially special secondary structure, excellent biocompatibility, and nontoxicity of degradation products [12]. Moreover, the polypeptide could be easily modified by functionalized PEG through chemical reactions. In this study, we developed two kinds of poly(L-glutamic acid)-cisplatin (PLG-Pt) nanocomplexes with detachable PEG that is responsive to tumor microenvironments, *e.g.*, low pH and matrix metalloproteinases-2/9 (MMP-2/9). The enhanced therapeutic effect could be achieved with these detachable PEGylated nanoformulations for high-grade serous ovarian cancer (HGSOC). As shown in Scheme 1, the bridged chemical bond between PEG and PLG was extracellular pH (pH_e)-responsive 2-propionic-3-methylmaleic anhydride (CDM)-derived amide bond [13] or MMP-cleaved peptide PLGLAG [14], corresponding to the graft copolymers PEG-pH_e-PLG or PEG-*MMP*-PLG, respectively. Cisplatin (CDDP), the most widely used first-line chemotherapeutic drug [15,16], was incorporated to the copolymers to form the polymer−metal complex nanoformulations, referred to as PEG-pH_e-PLG-Pt and PEG-*MMP*-PLG-Pt. The PEGylated PLG-CDDP nanoformulations showed prolonged blood circulation times and increased CDDP contents in the tumor tissue mediated by the EPR effect [12,17]. Upon accumulation in the tumor tissue, the acidic pH_e or

overexpressed MMP in the tumor microenvironments cleaved the bridged chemical bond between PEG and PLG. The released PLG-Pt had an enhanced cell uptake and upregulated antitumor efficacy. Compared with undetachable PEG-PLG-Pt, both PEG-pH_e-PLG-Pt and PEG-*MMP*-PLG-Pt with tumor microenvironment-responsive detachable PEGylation showed improved antitumor efficacies toward the HGSOC tumor model. Given the fascinating properties, the smart PLG-CDDP nanoformulations with detachable PEGylation exhibited promising prospects for clinical cancer therapy.

2. Materials and methods

2.1. Materials

γ-Benzyl-L-glutamate *N*-carboxyanhydride (BLG NCA), 3-benzyloxycarbonyl-L-lysine *N*-carboxyanhydride (ZLL NCA), and PEG-PLG were synthesized as described in our previous works [18,19]. BLG NCA and ZLL NCA were recrystallized twice from ethyl acetate before use. Methoxy poly(ethylene glycol) with M_n 5000 Da and *N*-hydroxysuccinimide (NHS) were obtained from Signa-Aldrich (Shanghai, P. R. China). *cis*-Diaminodichloroplatinum (II) was purchased from Shandong Boyuan Chemical Company (Jinan, P. R. China). CDM was purchased from Jilin Chinese Academy of Sciences-Yanshen Technology Co., Ltd. (Changchun, P. R. China). mPEG-SH with M_n = 5000 Da was purchased from Ponsure Biotechnology (Shanghai, P. R. China). MI-PLGLAG and 1-ethyl-3-(3-dimethylaminopropyl)carbodiimide hydrochloride (EDC·HCl) were purchased from GL Biochem (Shanghai, P. R. China) Ltd. *n*-Hexylamine, 33 wt% solution of HBr in acetic acid, and trifluoroacetic acid (TFA) were from Aladdin (Shanghai, P. R. China). All other reagents and solvents were purchased from Sinopharm Chemical Reagent Co. Ltd. (Shanghai, P. R. China) and used as received.
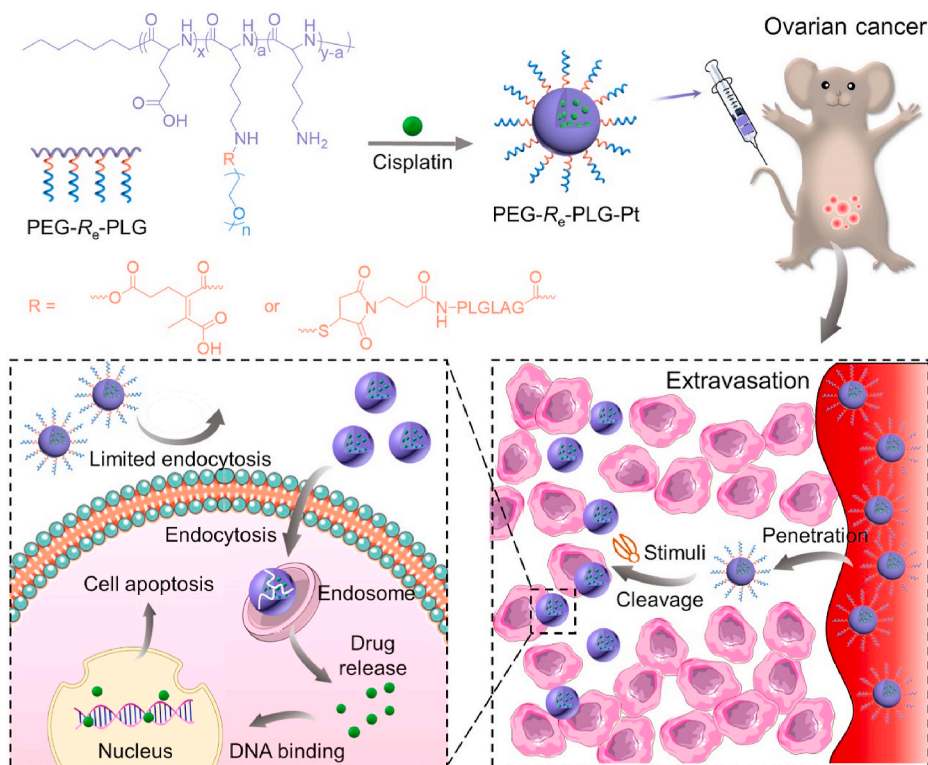
Scheme 1. Schematic illustration for preparation of PLG-CDDP nanoformulations with detachable PEG response to tumor microenvironments for enhanced therapy of peritoneal metastasis of ovarian cancer. Upon reaching the tumor tissue, dePEGylation is triggered by acidic pH or overexpression MMP, and the nanoformulations without PEG shell enter and deliver the drug to the cancer cells more effectively, leading to improving antitumor efficacy.

2.2. Synthesis of PEG-pH$_e$-PLG

PEG-pH_e-PLG was synthesized by the reaction between polypeptide and mPEG-CDM. Briefly, P(LG-*co*-LL) (0.41 g, 0.02 mmol) was dissolved in ice water and adjusted to pH 8.0 by adding sodium hydroxide (NaOH) aqueous solution. mPEG-CDM (1.04 g, 0.20 mmol) was added gradually to the P(LG-*co*-LL) solution, and the solution was maintained at pH 8.0 − 9.0 for 2 h adjusted by NaOH aqueous solution. The solution was moved into a dialysis bag (molecular weight cut-off (MWCO) = 14,000 Da) and dialyzed against NaOH aqueous solution at pH 8.0 − 9.0 for 24 h. Finally, PEG-pH_e-PLG was obtained after lyophilization.

2.3. Synthesis of PEG-MMP-PLG

PLGLAG, a MMP-sensitive cleavage peptide, was utilized to link PLG and mPEG for the synthesis of PEG-*MMP*-PLG. Briefly, mPEG-SH (1.00 g, 0.20 mmol) and MI-PLGLAG-COOH (0.15 g, 0.22 mmol) were dissolved in 20.0 mL of *N,N*-dimethylformamide (DMF) and stirred for 12 h. Then, EDC·HCl (126.5 mg, 0.66 mmol) and NHS (76.0 mg, 0.66 mmol) were added, and the reaction was maintained for 24 h. The solution was dialyzed against DMF to remove extra EDC·HCl and NHS. The solution of mPEG-PLGLAG-NHS was obtained and added gradually to the P(LG-*co*-LL) solution. The reaction was continued at room temperature for 24 h and then was moved into a dialysis bag (MWCO = 14,000 Da) and dialyzed against deionized water for 24 h. Finally, the solution was lyophilized, and PEG-*MMP*-PLG was obtained.

2.4. Assessment of pH$_e$- and MMP-responsiveness

The obtained PEG-pH_e-PLG was dissolved in deionized water, and pH was adjusted to 6.5 by using hydrochloric acid. At selected time intervals, 0.5, 2, 4, and 6 h, 1.0 mL of solution was taken out. The PEG content was determined by high-performance liquid chromatography (HPLC) analysis.

PEG-*MMP*-PLG (1.0 mg mL^{-1}) was incubated with 2.0 μg mL^{-1} MMP-2 in 25.0 mM *N*-2-hydroxyethylpiperazine-*N'*-2-ethanesulfonic acid (HEPES) buffer at pH 7.4 containing 5.0 mM calcium chloride (CaCl$_2$) at 37 °C. At selected time intervals, 0.5, 1, 2, and 4 h, 1.0 mL of solution was taken out and lyophilized. Then, the PEG content was detected by HPLC analysis.

2.5. Preparation of PLG-CDDP nanoformulations

The PLG-CDDP nanoformulations were prepared by the complexation of carboxyl group in the LG unit with CDDP in an aqueous solution. Typically, PLG, PEG-PLG, PEG-pH_e-PLG, or PEG-*MMP*-PLG (100.0 mg on a PLG equivalent) and 25.0 mg (0.083 mmol) of CDDP were dissolved in deionized water and shaken at 37 °C for 72 h. Free CDDP was removed by dialysis (MWCO = 3,500 Da) against NaOH aqueous solution at pH 8.0 − 9.0 for 24 h. The PLG-CDDP nanoformulations were obtained by lyophilization. The drug loading content (DLC) and drug loading efficiency (DLE) were calculated by the following equations.

$$DLC = \frac{\text{Weight of CDDP in PLG} - \text{CDDP nanoformulation}}{\text{Weight of PLG} - \text{CDDP nanoformulation}} \times 100\% \quad (1)$$

$$DLE = \frac{\text{Weight of CDDP in PLG} - \text{CDDP nanoformulation}}{\text{Weight of feeding CDDP}} \times 100\% \quad (2)$$

2.6. Pharmacokinetics

Female Sprague-Dawley rats were purchased from Beijing HFK Bioscience Co., Ltd. (Beijing, P. R. China) and randomly divided into five groups (*n* = 3; average weight: 180 g). CDDP, PLG-Pt, PEG-PLG-Pt, PEG-pH_e-PLG-Pt, or PEG-*MMP*-PLG-Pt was administered *via* the tail vein at an equivalent CDDP dose of 3.0 mg per kg body weight (mg (kg BW)$^{-1}$). At

predefined time points 5, 15, and 30 min, and 1, 3, 6, 12, and 24 h, 200.0 μL of blood samples were collected from the orbital cavities of rats, heparinized, and centrifuged (12,000 rpm, 5 min) to obtain plasma. Then, plasma samples were decomposed by heating with nitric acid, and the platinum contents were determined by inductively coupled plasma-mass spectrometry (ICP-MS, NexION, PerkinElmer, USA). All of the data obtained by ICP-MS were analyzed using the PKSolver program (China Pharmaceutical University, Nanjing, P. R. China) [20].

2.7. Biodistribution

To investigate the biodistribution of free CDDP and PLG-CDDP nanoformulations in the peritoneal metastasis of ovarian cancer xenografted nude mouse, female BALB/c nude mice (*n* = 3; 18 − 20 g, 5 − 6 weeks) were inoculated intraperitoneally with 5.0×10^6 SKOV3 cells. After seven days, CDDP or various PLG-CDDP nanoformulations was administered intravenously at a dose of 3.0 mg (kg BW)$^{-1}$ on a CDDP equivalent. The mice were sacrificed at 24 h after injection. The heart, liver, spleen, lung, kidney, and tumor were excised. Then, the tissues were decomposed by heating with nitric acid, and the platinum concentration in the solution was measured by ICP-MS.

2.8. In vivo antitumor efficacy

The antitumor efficacies of free CDDP and PLG-CDDP nanoformulations were assessed toward the peritoneal metastasis of ovarian cancer xenografted nude mouse. The female BALB/c nude mice (18 − 20 g, 5 − 6 weeks) were bought from Charles River Laboratories (Beijing, P. R. China). All animals received care in compliance with the guidelines outlined in the "Guide for the Care and Use of Laboratory Animals", and all procedures were approved by the Animal Care and Use Committee of Institute of Chemistry, Chinese Academy of Sciences (Beijing, P. R. China). The mice were intraperitoneally injected with the LUC$^+$/RFP$^+$ OVCAR8 cells at a dosage of 1.5×10^6 cells per mouse to establish the HGSOC model [21]. Then, the mice were randomly divided into six groups (*n* = 5) and intravenously injected with phosphate-buffered saline (PBS), CDDP, PLG-Pt, PEG-PLG-Pt, PEG--pH_e-PLG-Pt, or PEG-*MMP*-PLG-Pt at an equivalent CDDP concentration of 3.0 mg (kg BW)$^{-1}$ every four days. Luciferase signals of the tumors in each group were imaged *in vivo* periodically. Changes in signal intensities determined by measuring the average photon flux in radians were compared to baseline, enabling normalization for differences in imaging area between mice and in the same mouse over time. The body weight of mouse was also recorded every four days. At the end of treatment, the mice were sacrificed, and normal organs, *i.e.*, the heart, liver, spleen, lung and kidney, and tumor were collected for histopathological analysis.

2.9. Statistical analysis

All experiments were performed as means ± standard deviation (SD). Data were analyzed for statistical significance using SPSS 21.0 (SPSS Inc., Chicago, IL, USA). *$P < 0.05$ was considered statistically significant, and **$P < 0.01$ and ***$P < 0.001$ were considered highly significant.

3. Results and discussion

3.1. Synthesis and characterizations of PEG-pH$_e$-PLG and PEG-MMP-PLG

The synthesis routes of PEG-pH_e-PLG and PEG-*MMP*-PLG were shown in Supplementary Fig. S1. Polypeptides were synthesized by the ring-opening polymerization (ROP) of α-amino acid NCA monomers initiated by various amino groups, according to the protocols described in our previous studies [19,22]. Poly(γ-benzyl-ʟ-glutamate-*co-N*

(ε)-benzyloxycarbonyl-L-lysine) (P(BLG-*co*-ZLL)) was synthesized by the ROP of BLG NCA and ZLL NCA using *n*-hexylamine as an initiator, and poly(L-glutamic acid-*co*-L-lysine) (P(LG-*co*-LL) was obtained through the deprotection of P(BLG-*co*-ZLL) with hydrogen bromide solution, 33 wt% in acetic acid [23]. The signals of proton nuclear magnetic resonance (^{1}H NMR) spectra for various polymers were shown in Supplementary Table S1. The successful synthesis of P(BLG-*co*-ZLL) and P(LG-*co*-LL) were demonstrated by ^{1}H NMR, as shown in Supplementary Fig. S2, and Fig. 1A. Furthermore, the polymerization degrees of LG and LL were calculated to be 149 and 10, responsively.

Thereafter, PEG-PLG was synthesized by the condensation reaction between the carboxyl group in the LG unit and the terminal hydroxyl group of mPEG according to the protocol reported in our previous work (Supplementary Fig. S1) [24]. PEG was successfully modified to be mPEG-CDM after the synthesis of chlorine-substituted CDM through the reaction between the CDM and oxalyl chloride, as shown in Supplementary Fig. S3 [13]. The characteristic resonances at 2.14 and 2.76 ppm belonged to the methyl protons (a) and methylene protons (b) of CDM, and the signal at 4.24 ppm ($-OCH_2CH_2OC(O)-$, e) proved the successful synthesis of mPEG-CDM. PEG-*pH*$_e$-PLG was synthesized by the ring-opening reaction between the anhydride group in mPEG-CDM and the amino group in the LL unit of P(LG-*co*-LL). The signal at 3.58 ppm in ^{1}H NMR spectra proved the existence of PEG, indicating the successful synthesis of PEG-*pH*$_e$-PLG.

For the preparation of PEG-*MMP*-PLG, mPEG-PLGLAG-COOH was first synthesized by the Michael addition reaction between the terminal thiol group in mPEG-SH and maleimide (MI) group in the functional peptide MI-PLGLAG-COOH. Then, mPEG-PLGLAG-COOH was activated by NHS catalyzed by EDC·HCl to synthesize mPEG-PLGLAG-NHS.

Finally, PEG-*MMP*-PLG was synthesized by the reaction between the NHS-activated carboxyl group in mPEG-PLGLAG-NHS and the amino group in the LL unit of P(LG-*co*-LL). The successful preparation of PEG-*MMP*-PLG was proved by the signal of PEG at 3.58 ppm in ^{1}H NMR spectra.

In addition, the synthesis of polypeptide was also confirmed by the appearance of typical amide bonds at 1654 cm^{-1} ($\nu_{C=O}$) and 1548 cm^{-1} ($\nu_{C(O)-NH}$) in Fourier-transform infrared (FT−IR) spectra (Supplementary Fig. S4). Meanwhile, the absorption peak of C–H bonds appeared at 2753 cm^{-1} in FT-IR spectra, indicating the existence of PEG. Furthermore, the grafting density of PEG was examined by ^{1}H NMR and gel filtration chromatography (GFC) (Supplementary Table S2). The molar ratio of Glu unit and PEG monomer unit and M_n of PEG-PLG, PEG-*pH*$_e$-PLG, and PEG-*MMP*-PLG were very close, proving similar grafting density.

According to our design, tumor microenvironment could lead to the PEG deshielding from PEG-*pH*$_e$-PLG and PEG-*MMP*-PLG. To confirm this hypothesis, the PEG release behavior was detected by HPLC. The PEG peak was exhibited at an elution time at 16.7 min. PEG-*pH*$_e$-PLG showed a rapid PEG release at pH 6.5, with a nearly 80% of cumulative release within 4 h (Fig. 1B). Similarly, the MMP-2-sensibility of PEG-*MMP*-PLG was also detected by HPLC after coincubation with MMP-2.76.8% of the linker was cleaved within 2 h (Fig. 1C). The above data demonstrated that the pH- and MMP-sensitive linkages between polypeptide and mPEG could be efficiently cleaved in the specific microenvironments of tumor tissue.
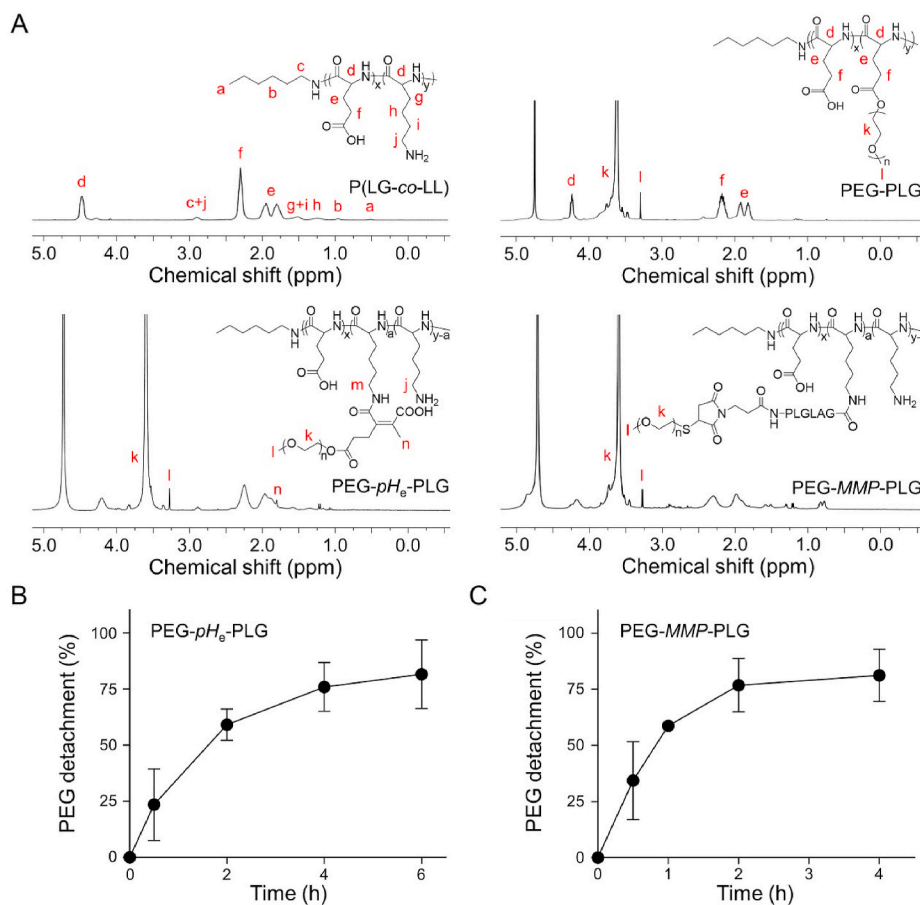

Fig. 1. Characterizations of P(LG-*co*-LL), PEG-PLG, PEG-*pH*$_e$-PLG, and PEG-*MMP*-PLG. (A) ^{1}H NMR spectra of PLG, PEG-PLG, PEG-*pH*$_e$-PLG, and PEG-*MMP*-PLG. (B) PEG detachment kinetics from PEG-*pH*$_e$-PLG at pH 6.5. (C) PEG detachment kinetics from PEG-*MMP*-PLG in presence of MMP-2. The statistical data are represented as mean ± standard deviation (SD; $n = 3$).

3.2. Preparation and characterizations of PLG-CDDP nanoformulations

To exploit the benefits of a detachable PEGylation strategy for cancer therapy, CDDP was incorporated to the copolymers to form nanoformulations. The PLG has abundant carboxyl groups in the LG units that are able to form complex with Pt(II) in CDDP to prepare various polymer−metal complex nanoformulations. According to this protocol, various PLG-CDDP nanoformulations, including PLG-Pt, PEG-PLG-Pt, PEG-pH_e-PLG-Pt, or PEG-*MMP*-PLG-Pt, were prepared through the ligand exchange reaction between P(LG-*co*-LL), PEG-PLG, PEG-pH_e-PLG, or PEG-*MMP*-PLG and CDDP in aqueous solution, respectively [25,26]. The DLCs and DLEs of CDDP in the above nanoformulations were provided in Supplementary Table S3, which proved the efficient and close CDDP-loaded capacity of various copolymers.

The hydrodynamic diameters (D_hs) of PLG-CDDP nanoformulations were examined by dynamic laser scattering (DLS) in intensity model, which were 9.2 ± 1.6, 13.2 ± 3.3, 12.6 ± 3.6, and 14.2 ± 4.0 nm, respectively, as shown in Fig. 2A and Supplementary Table S3. The size distributions of different PLG-CDDP nanoformulations were appropriate to the required scale ranges for passive tumor targeting by the EPR effect [27,28]. The ζ potentials of PLG-Pt, PEG-PLG-Pt, PEG-pH_e-PLG-Pt, and PEG-*MMP*-PLG-Pt were -27.2 ± 2.1, -17.9 ± 2.5, -16.5 ± 0.6, and -15.5 ± 1.3 mV, respectively. Compared with PLG-Pt, the increased ζ potentials of PEG-PLG-Pt, PEG-pH_e-PLG-Pt, and PEG-*MMP*-PLG-Pt should be attributed to the modification of PEG, which decreased the density of LG unit in the polypeptide chain. The negative charges favored the prolonged circulation times of PLG-CDDP nanoformulations.

In order to examine the drug release behavior of nanoformulations *in vitro*, CDDP release in PBS at pH 7.4, 6.8, or 5.5 with or without previous pre-incubation with MMP-2 was detected by the dialysis method. As shown in Fig. 2B, none of the PLG-CDDP nanoformulations showed an initial burst release of CDDP within 24 h. Less than 30% of CDDP was released from PLG-CDDP nanoformulations at pH 7.4 within 72 h. The sustained release behaviors of PLG-CDDP nanoformulations were similar to our finding in the previous report [24]. It was owing to the stable coordination between CDDP and the carboxylate groups of PLG moiety at pH 7.4. Meanwhile, the cumulative release of CDDP from PLG-CDDP nanoformulations could be accelerated by decreasing pH from 7.4 to 6.5 and 5.5. Typically, the amount of drug release from PLG-Pt, PEG-PLG-Pt, PEG-pH_e-PLG-Pt, and PEG-*MMP*-PLG-Pt at 72 h reached 78.8%, 58.4%, 69.6%, and 55.2% at pH 5.5, respectively. The

higher release rate of CDDP in acidic conditions should be attributed to the stronger protonation of free carboxylic groups of PLG at acidic pH, which weakened CDDP and PLG-CDDP nanoformulations coupling [29]. A higher percentage of CDDP was released from PEG-pH_e-PLG-Pt compared with PEG-PLG-Pt at pH 5.5. Meanwhile, pre-incubation with MMP-2 solution resulted in faster drug release from PEG-*MMP*-PLG-Pt than that without MMP-2 pre-incubation. These data demonstrated that dePEGylation caused by acidic or MMP-2 cleavage led to rapid CDDP release from PLG-CDDP nanoformulations. This finding was similar to other reported studies [30]. All these data demonstrated that the PEG-pH_e-PLG-Pt and PEG-*MMP*-PLG-Pt could reduce the CDDP release in blood circulation and achieve effective and controlled drug release in tumor tissue.

3.3. In vitro cell uptake and toxicity of various PLG-CDDP nanoformulations

After dePEGylation, the released PLG-Pt, which should have better cell uptake ability, is expected to increase CDDP concentration in cancer cells. To demonstrate this assumption, the intracellular internalization of free CDDP and PLG-CDDP nanoformulations toward SKOV3 cells and LUC$^+$/RFP$^+$ OVCAR8 cells was investigated by a confocal laser scanning microscope (CLSM) (Fig. 3A). In order to observe the cell uptake behaviors, the PLG-CDDP nanoformulations were labeled with FITC. As shown in Fig. 3A, the PEG-PLG-Pt showed the weakest signal of intracellular FITC fluorescence in SKOV3 cells compared with other groups. This was because of the limited cell endocytosis caused by the steric interactions between grafted PEG chains and the cell membrane. Meanwhile, compared with PEG-PLG-Pt, PEG-pH_e-PLG-Pt showed a similar cell uptake at pH 7.4, and a higher cell uptake at pH 6.5. This was because the CDM-derived amide bond between PEG chains and PLG was stable at pH 7.4 but was cleaved at pH 6.5. After dePEGylation, the remaining uncoated PLG-Pt core showed an enhanced cell uptake and CDDP release efficacy. Similarly, due to the overexpressed MMP-2 in the ovarian cell line [31], PEG-*MMP*-PLG-Pt also showed a higher uptake and CDDP content than PEG-PLG-Pt. More cellular uptake leads to higher drug content. As expected, the free CDDP group showed the highest CDDP content in SKOV3 cells (Fig. 3B). This was because the cell uptake of PLG-CDDP nanoformulations was achieved *via* the endocytosis pathway, while free CDDP entered cells *via* diffusion [27]. Meanwhile, there were higher CDDP contents of PEG-pH_e-PLG-Pt and
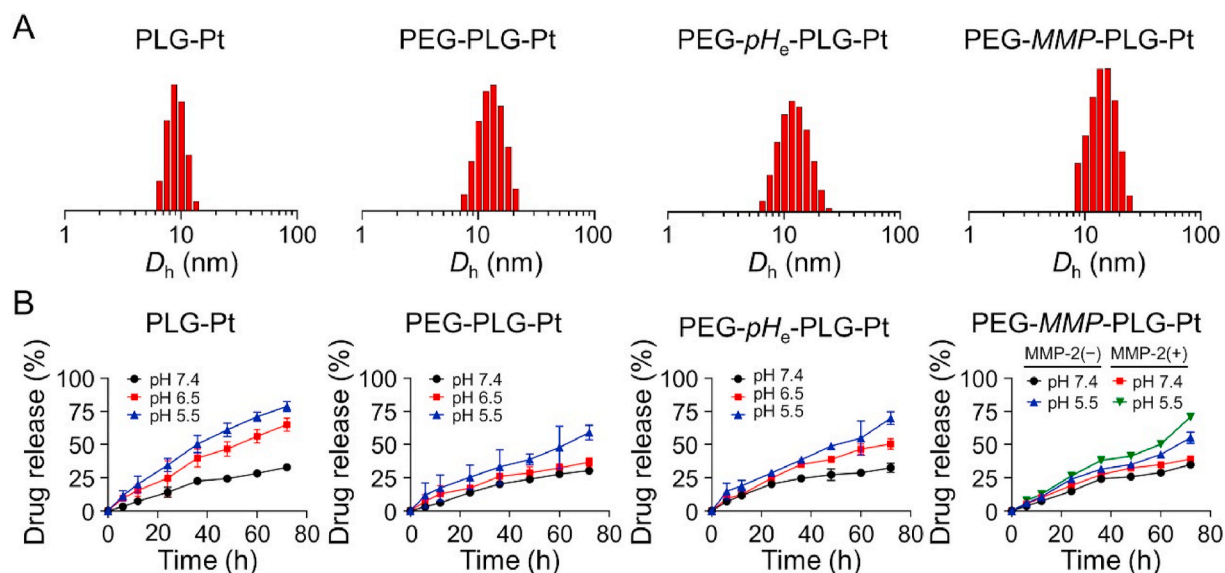

Fig. 2. Characterizations of PLG-Pt, PEG-PLG-Pt, PEG-pH_e-PLG-Pt, and PEG-*MMP*-PLG-Pt. (A) D_hs of PLG-Pt, PEG-PLG-Pt, PEG-pH_e-PLG-Pt, and PEG-*MMP*-PLG-Pt. Scale bar indicates 50 nm. (B) CDDP release profiles from PLG-CDDP nanoformulations. The statistical data are represented as mean ± standard deviation (SD; $n = 3$).
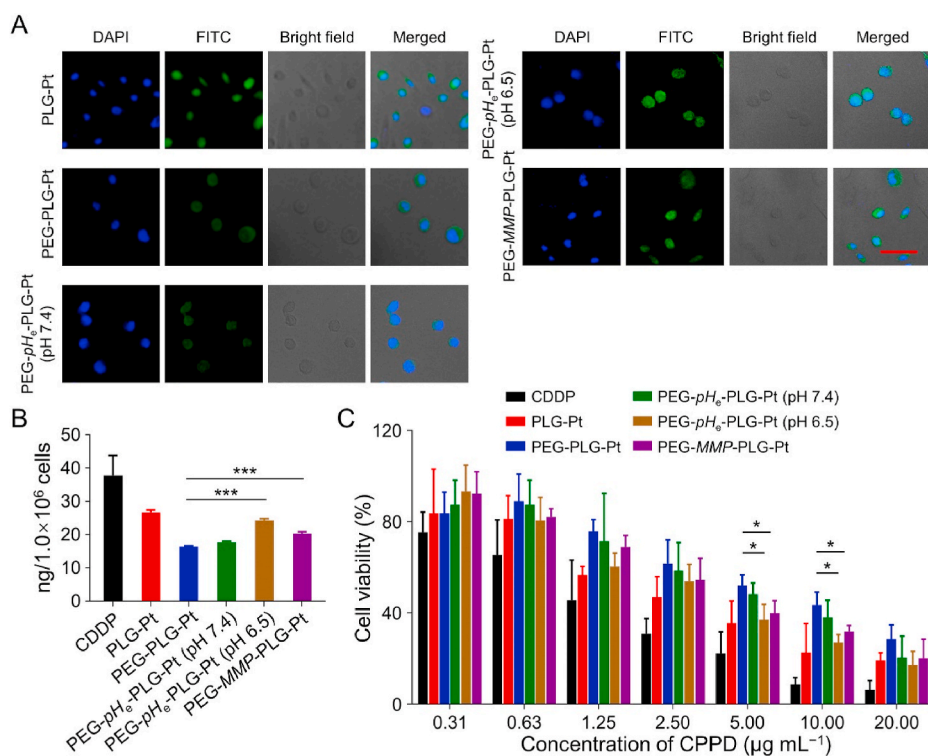
PEG-*MMP*-PLG-Pt compared with PEG-PLG-Pt group due to the dePEGylation. Furthermore, the enhanced cell uptake and increased intracellular CDDP content of PEG-*pH*e-PLG-Pt and PEG-*MMP*-PLG-Pt were also determined in LUC$^+$/RFP$^+$ OVCAR8 cells (Supplementary Fig. S5 and Fig. S6), which were consistent with those of SKOV3 cells. The endocytosis of nanoformulations was affected by many factors, such as size, ζ-potential, secondary structure of PLG (α-helix and β-sheet), and PEGylation [32–34]. However, the PEGylation is likely to be the main factor affecting endocytosis in our study, because the main difference among nanoformulations was the bridged chemical bond between PLG and PEG. All results confirmed that the PLG-CDDP nanoformulations with detachable PEGylation had enhanced cell uptake and intracellular CDDP content.

The increased accumulation of CDDP in cancer cells was beneficial in terms of improving anti-proliferation activity. Thus, the cell viability was evaluated by Alamar blue assay in SKOV3 cells with different concentrations of polypeptides or PLG-CDDP nanoformulations. In Supplementary Fig. S7, cancer cells treated with polypeptides for 48 h showed viabilities of around 100% even at high concentrations, revealing outstanding biocompatibility of the copolymers to cells. Furthermore, the *pH*- and *MMP*-responsive PEG-*R*e-PLG-CDDP nanoformulations showed more potent antitumor efficacy than non-responsive ones at the same CDDP concentration (Fig. 3C). The half-maximal inhibitory concentration (IC$_{50}$) values of free CDDP, PLG-Pt, PEG-PLG-Pt, PEG-*pH*e-PLG-Pt (pH 7.4), PEG-*pH*e-PLG-Pt (pH 6.5), and PEG-*MMP*-PLG-Pt were 1.2, 4.8, 11.0, 8.5, 5.8 and 6.9 μg mL^{-1}, respectively (Supplementary Table S4). The cytotoxicities of PEG-*pH*e-PLG-Pt and PEG-*MMP*-PLG-Pt were higher than that of PEG-PLG-Pt. It was because dePEGylation of PLG-CDDP nanoformulations, which led to enhanced cell uptake and faster CDDP release. Meanwhile, the cytotoxicity of various PLG-CDDP nanoformulations was also evaluated in LUC$^+$/RFP$^+$ OVCAR8 cells. Similarly, all polypeptide groups showed no apparent toxicity even at high concentrations (Supplementary Fig. S8). The PEG-PLG-Pt, PEG-*pH*e-PLG-Pt (pH 7.4), PEG-*pH*e-PLG-Pt (pH 6.5), and PEG-*MMP*-PLG-Pt had IC$_{50}$ values of 10.6, 7.6 4.0, and 5.3 μg mL^{-1}, respectively (Supplementary Fig. S9), similar to the results in SKOV3 cells. These findings

indicated that the PLG-CDDP nanoformulations with detachable PEG resulted in enhanced cytotoxicity due to effective cell uptake and rapid intracellular CDDP release.

3.4. In vivo pharmacokinetics and biodistribution of CDDP

The evaluation of pharmacokinetics is a crucial step to enter the clinical study. The pharmacokinetics of free CDDP and various PLG-CDDP nanoformulations were evaluated by single tail vein injection into healthy rats (3.0 mg (kg BW)$^{-1}$ on a CDDP basis). The serum was collected at the selected time points and decomposed on heating in nitric acid before determining platinum contents by ICP-MS. The mean serum concentration-time curves of platinum were shown in Fig. 4A. The half-lives ($t_{1/2}$) of CDDP, PLG-Pt, PEG-PLG-Pt, PEG-*pH*e-PLG-Pt, and PEG-*MMP*-PLG-Pt groups were 0.4, 1.9, 8.8, 7.9, and 7.8 h, respectively. Meanwhile, the drug concentration-time curves (AUC$_{0-t}$) were 23.0, 92.7, 460.1, 407.7, and 363.0 h μg mL^{-1}, respectively (Supplementary Table S4). As expected, the free CDDP groups showed the shortest $t_{1/2}$ and lowest AUC$_{0-t}$ values, owing to rapid clearance *in vivo*. The PEG-PLG-Pt, PEG-*pH*e-PLG-Pt, and PEG-*MMP*-PLG-Pt showed higher $t_{1/2}$ and AUC$_{0-t}$ values as compared with PLG-Pt. These results were consistent with our previous work [18,24]. Meanwhile, compared with PEG-PLG-Pt, PEG-*pH*e-PLG-Pt, and PEG-*MMP*-PLG-Pt showed slightly smaller $t_{1/2}$ and AUC$_{0-t}$ values. It could be explained that the *pH*e-responsive CDM-derived amide bond and *MMP*-responsive PLGLAG peptide was less stable *in vivo* compared with the ester bond in PEG-PLG. Overall, these results indicated that the PEG chain on the particle surface could prolong the circulation time by providing a shield for nanoparticles from rapid clearance by the organism and increased the opportunity to accumulate in tumor tissue through the EPR effect.

The distribution of antitumor agents is influential to their therapeutic efficacy and toxicity to normal organs [35,36]. The biodistribution of free CDDP and PLG-CDDP nanoformulations was detected in tumor-bearing mice. Seven days after intraperitoneal injection of SKOV3 cells, free CDDP or other nanoformulations was injected through the tail vein. After 24 h, major organs (heart, liver, spleen, lung,
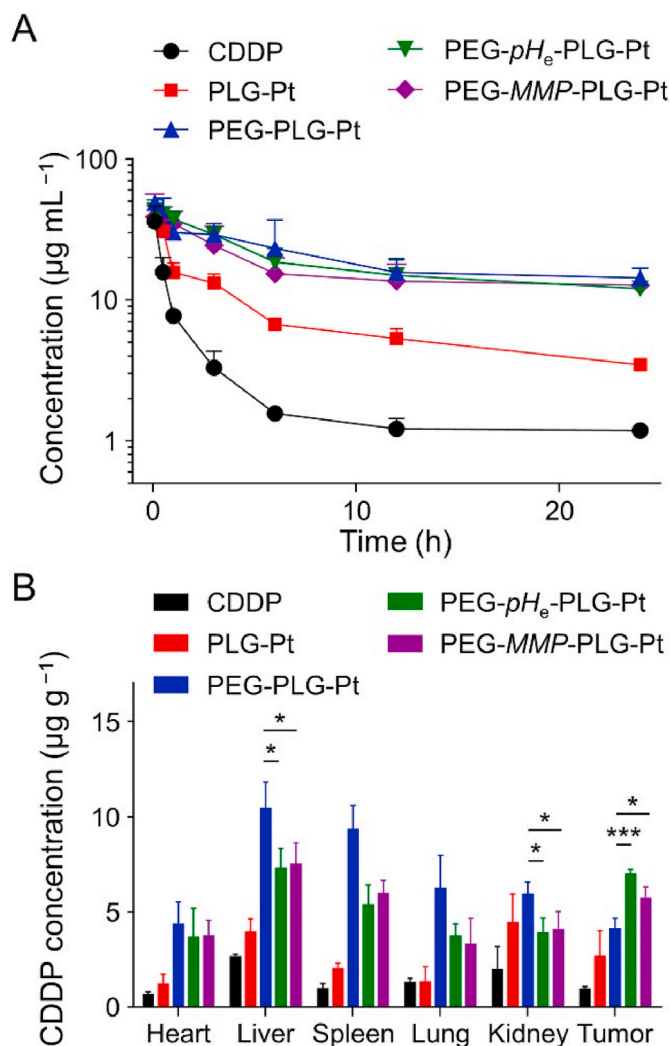
Fig. 4. *In vivo* pharmacokinetics and biodistribution of CDDP, PLG-Pt, PEG-PLG-Pt, PEG-pH_e-PLG-Pt, and PEG-MMP-PLG-Pt. (A) Pharmacokinetics of CDDP and PLG-CDDP nanoformulations after intravenous injection into Sprague-Dawley rats. (B) Concentrations of CDDP in organs (the heart, liver, spleen, lung, and kidney) and tumors at 48 h post-injection. The statistical data are represented as mean $\pm$ SD ($n = 3$; *$P < 0.001$, ***$P < 0.001$).

and kidney) and tumors were collected and decomposed on heating in nitric acid to detect platinum content by ICP-MS. As shown in Fig. 4B, PEGylated PLG-CDDP nanoformulations showed an increased CDDP concentration in each organ compared with free CDDP and PLG-Pt within 24 h after intravenous injection, which was due to their enhanced circulation times *in vivo* [18]. In addition, the PEG-pH_e-PLG-Pt and PEG-MMP-PLG-Pt showed reduced accumulation in normal organs and 1.7- and 1.4-folds higher accumulation in tumor tissue compared with PEG-PLG-Pt, respectively, indicating the enhanced antitumor effect and reduced side effects. It was because the tumor microenvironment-responsive detachable PEGylated PLG-CDDP nanoformulations facilitated the retention in tumor tissue. Upon accumulation in tumor tissue, the acidic pH_e or overexpressed MMP in the tumor microenvironment cleaved the bridged chemical bond between PEG and PLG, and the PLG-CDDP nanoformulations without PEG chain showed enhanced cellular uptake. Overall, the PEG-pH_e-PLG-Pt and PEG-MMP-PLG-Pt with enhanced drug retention in the tumor tissue exhibited the advantageous drug-delivery performance.

3.5. In vivo antitumor efficiency

The antitumor efficiencies of CDDP-loaded PLG-CDDP nanoformulations were evaluated in nude mice bearing disseminated LUC$^+$/RFP$^+$ OVCAR8 ovarian cancer. 15 days after the injection of cancer cells, the mice were injected *via* tail vein with PBS, free CDDP, or various PLG-CDDP nanoformulations (3.0 mg (kg BW)$^{-1}$ on a CDDP basis) every four days. The tumors in mice were monitored every seven days by *in vivo* imaging system. The luminescent signal intensities emanating from the tumors of each group confirmed the antitumor activity [37]. As expected, the PEG-PLG-Pt group showed an obvious antitumor effect and extended survival time compared to the free CDDP and PLG-Pt groups (Fig. 5 and Supplementary Fig. S10). This can be attributed to the prolonged circulation time and sustained drug release in the tumor tissue of PEGylated PLG-CDDP nanoformulations, which was also proved in our previous works [18,24]. Meanwhile, PEG-pH_e-PLG-Pt and PEG-MMP-PLG-Pt exhibited better antitumor efficiency and extended survival time in comparison with the PEG-PLG-Pt group. The improved therapeutic effects of PEG-detachable nanoformulations were in accordance with their enhanced tumor accumulation and effective cell uptake owning to their stimuli-responsive dePEGylation in tumor tissue.

The histological analysis supported the enhanced therapeutic effect described in Fig. 5D and Supplementary Fig. S11. As expected, compared with other groups, PEGylated PLG-CDDP nanoformulations showed a larger area of necrosis with morphological features by hematoxylin and eosin (H&E) staining. Meanwhile, there were also more active-caspase-3-positive apoptotic cells and fewer PCNA-positive proliferating cells confirmed by immunohistochemical studies. In addition, the PEG-pH_e-PLG-Pt and PEG-MMP-PLG-Pt with the most potent antitumor effect could be observed among PEGylated PLG-CDDP, which was consistent with the result of antitumor efficacy. The above findings verified that detachable PEGylated nanoformulations could achieve superior anticancer efficacy.

In addition, the PEGylated PLG-CDDP nanoformulations showed reduced systemic toxicity of free CDDP. As shown in Supplementary Fig. S12, the body weight decreased in the CDDP group, while the body weights remained almost unchanged in PEG-pH_e-PLG-Pt and PEG-MMP-PLG-Pt groups, further suggesting the increased systemic safety. Hence, the PEG-pH_e-PLG-Pt and PEG-MMP-PLG-Pt are promising platforms in cancer treatment.

4. Conclusion

PEGylated PLG-CDDP nanoformulations significantly prolong the circulation time in the blood and increase drug accumulation in the tumor tissue. However, PLG-CDDP nanoformulations with PEG chains showed limited cell uptake and bioavailability, which reduced the therapeutic potential of nanomedicines. In this study, we developed two tumor microenvironment-responsive detachable CDDP-loaded PEGylated PLG complex nanoformulations, PEG-pH_e-PLG-Pt and PEG-MMP-PLG-Pt, whose bridged chemical bond was pH_e-responsive CDM-derived amide bond or MMP-2-responsive PLGLAG, respectively. The CDDP-loaded pH_e- and MMP-responsive PEGylated PLG-CDDP nanoformulations with diameters of 12.6 $\pm$ 3.6 nm, and 14.2 $\pm$ 4.0 nm, respectively, showed prolonged blood circulation, evidenced by increased $t_{1/2}$ and AUC$_{0-t}$. Upon accumulation in tumor tissue, the acidic pH_e or overexpressed MMP at the tumor microenvironment cleaved the bridged chemical bond between PEG and PLG. The PLG-CDDP nanoformulations without PEG shell had enhanced cell uptake and cytotoxicity. Furthermore, PEG-pH_e-PLG-Pt and PEG-MMP-PLG-Pt, especially the former oner, showed enhanced inhibition efficacy and survival rate *in vivo*. Therefore, the tumor microenvironment-induced detachable CDDP-loaded PEGylated PLG complex nanoformulations provided an effective strategy for designing CDDP nanomedicines.
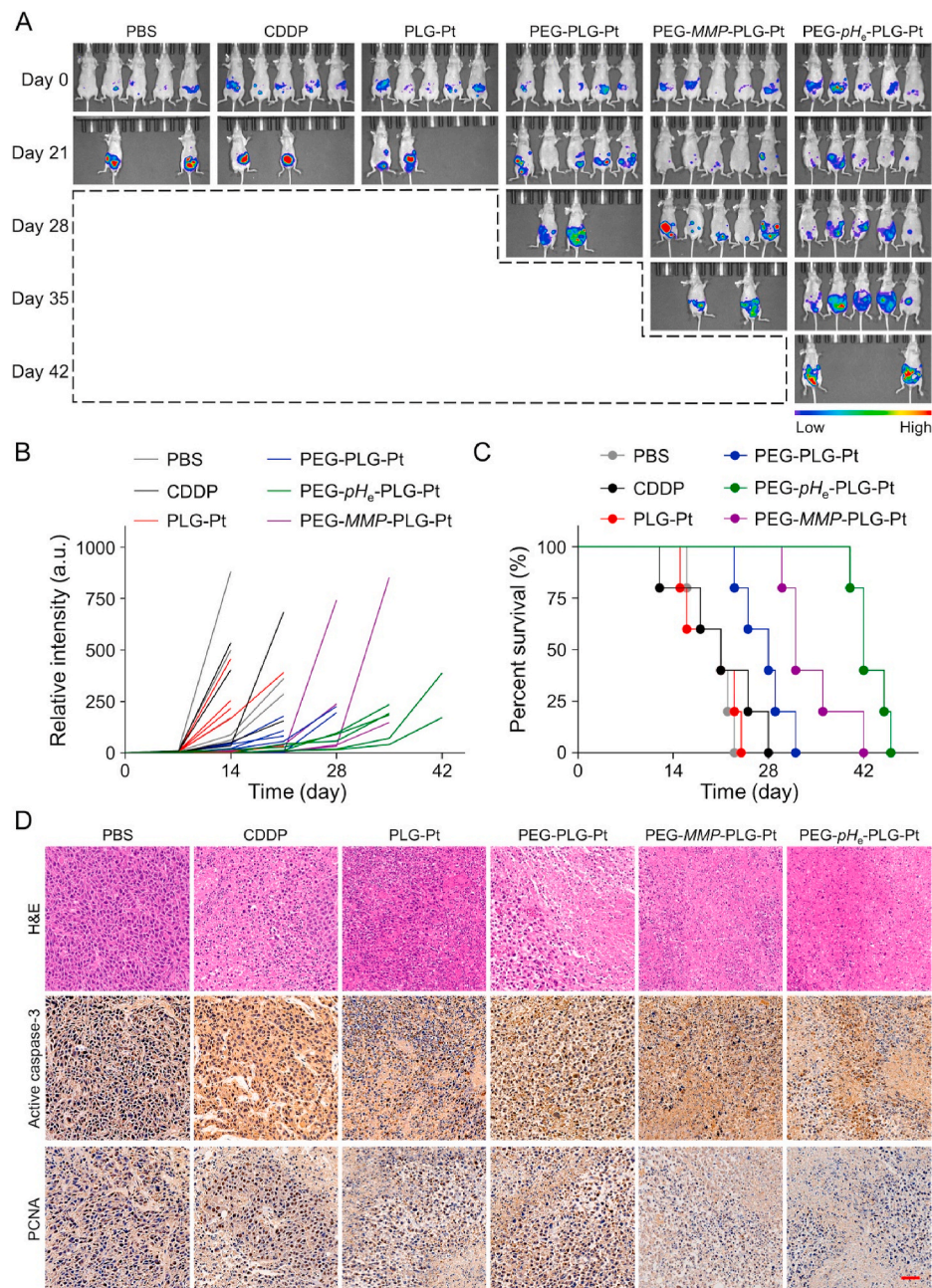
Fig. 5. *In vivo* antitumor efficacy of CDDP and various PLG-CDDP nanoformulations. (A) Bioluminescent imaging of mice with HGSOC at different time points. (B) Relative luciferase intensity in tumor region analyzed from bioluminescent imaging. (C) Survival of mice in different treatment groups. (D) Hematoxylin and eosin (H&E), active caspase-3, and proliferating cell nuclear antigen (PCNA)-staining of tumor tissues from mice in different treatment groups. Scale bar indicates 50 μm.

Data availability

All relevant data supporting the findings of this study are either included within the article and its Supplementary Information files or available upon request from the corresponding author.

CRediT authorship contribution statement

Zhongyu Jiang: Conceptualization, Methodology, Writing - original draft. **Xiangru Feng:** Investigation, Writing - original draft. **Haoyang Zou:** Methodology. **Weiguo Xu:** Conceptualization, Supervision, Writing - review & editing. **Xiuli Zhuang:** Resources, Supervision, Writing - review & editing.

Declaration of competing interest

The authors declare that they have no known competing financial interests or personal relationships that could have appeared to influence the work reported in this paper.

Acknowledgments

Appendix A. Supplementary data

Supplementary data to this article can be found online at https://doi.org/10.1016/j.bioactmat.2021.01.034.

List of abbreviations

^{1}H NMR	proton nuclear magnetic resonance
AUC$_{0-t}$	area under the drug concentration-time curve
BLG NCA	γ-benzyl-L-glutamate *N*-carboxyanhydride
CaCl$_2$	calcium chloride
CDDP	cisplatin, *cis*-diaminodichloroplatinum (II)
CDM	2-propionic-3-methylmaleic anhydride
CLSM	confocal laser scanning microscope
D_hs	hydrodynamic diameters
DLC	drug loading content
DLE	drug loading efficiency
DLS	dynamic laser scattering
DMF	*N,N*-dimethylformamide
EDC·HCl	1-ethyl-3-(3-dimethylaminopropyl)carbodiimide hydrochloride
EPR effect	enhanced permeability and retention effect
FT-IR	Fourier-transform infrared
GFC	gel filtration chromatography
H&E	hematoxylin and eosin
HEPES	*N*-2-hydroxyethylpiperazine-*N′*-2-ethanesulfonic acid
HGSOC	high-grade serous ovarian cancer
HPLC	high-performance liquid chromatography
IC$_{50}$	half-maximal inhibitory concentration
ICP-MS	inductively coupled plasma-mass spectrometry
MI	maleimide
MMP-2/9	matrix metalloproteinases-2/9
M_n	number-average molecular weight
MWCO	molecular weight cut-off
NaOH	sodium hydroxide
NHS	*N*-hydroxysuccinimide
P(LG-*co*-LL)	poly(L-glutamic acid-*co*-L-lysine)
PCNA	proliferating cell nuclear antigen
PEG	poly(ethylene glycol)
PEG-*MMP*-PLG	matrix metalloproteinases -responsive poly(L-glutamic acid)-*g*-methoxy poly(ethylene glycol)
PEG-*MMP*-PLG-Pt	matrix metalloproteinases -responsive poly(L-glutamic acid)-*g*-methoxy poly(ethylene glycol)-cisplatin
PEG-*pH*$_e$-PLG	extracellular pH-responsive poly(L-glutamic acid)-*g*-methoxy poly(ethylene glycol)
PEG-*pH*$_e$-PLG-Pt	extracellular pH -responsive poly(L-glutamic acid)-*g*-methoxy poly(ethylene glycol)-cisplatin
PEG-PLG	poly(L-glutamic acid)-*g*-methoxy poly(ethylene glycol)
PEG-PLG-Pt	poly(L-glutamic acid)-*g*-methoxy poly(ethylene glycol)-cisplatin
pH$_e$	extracellular pH
PLG-Pt	poly(L-glutamic acid)-cisplatin
P(BLG-*co*-ZLL)	poly(γ-benzyl-L-glutamate-*co*-N(ε)-benzyloxycarbonyl-L-lysine)
$t_{1/2}$	half-life
TFA	trifluoroacetic acid
ZLL NCA	3-benzyloxycarbonyl-L-lysine *N*-carboxyanhydride

References

[1] L. Kong, F. Campbell, A. Kros, DePEGylation strategies to increase cancer nanomedicine efficacy, Nanoscale Horiz 4 (2019) 378–387.

[2] D. Wu, M. Qin, D. Xu, L. Wang, C.Y. Liu, J. Ren, G. Zhou, C. Chen, F.M. Yang, Y.Y. Li, Y. Zhao, R.Y. Huang, S. Pourtaheri, C.S. Kang, M. Kamata, I.S.Y. Chen, Z. L. He, J. Wen, W. Chen, Y.F. Lu, A bioinspired platform for effective delivery of protein therapeutics to the central nervous system, Adv. Mater. 31 (2019) 1807557.

[3] Q. Yang, S.K. Lai, Anti-PEG immunity: emergence, characteristics, and unaddressed questions, Wiley Interdiscip. Rev.: Nanomed. Nanobiotechnol. 7 (2015) 655–677.

[4] J.S. Suk, Q.G. Xu, N. Kim, J. Hanes, L.M. Ensign, PEGylation as a strategy for improving nanoparticle-based drug and gene delivery, Adv. Drug Deliv. Rev. 99 (2016) 28–51.

[5] G.C. Yu, T.Y. Cen, Z.M. He, S.P. Wang, Z.T. Wang, X.W. Ying, S.J. Li, O. Jacobson, S. Wang, L. Wang, L.S. Lin, R. Tian, Z.J. Zhou, Q.Q. Ni, X.P. Li, X.Y. Chen, Porphyrin nanocage-embedded single-molecular nanoparticles for cancer nanotheranostics, Angew. Chem. Int. Ed. 58 (2019) 8799–8803.

[6] C.Y. Yin, S.H. Wang, Q.Z. Ren, X.M. Shen, X.D. Chen, Y.J. Liu, S.J. Liu, Radial extracorporeal shock wave promotes the enhanced permeability and retention effect to reinforce cancer nanothermotherapeutics, Sci. Bull. 64 (2019) 679–689.

[7] Q.H. Sun, Z.X. Zhou, N.S. Qiu, Y.Q. Shen, Rational design of cancer nanomedicine: nanoproperty integration and synchronization, Adv. Mater. 29 (2017) 1606628.

[8] P. Mi, H. Cabral, K. Kataoka, Ligand-installed nanocarriers toward precision therapy, Adv. Mater. 32 (2020) 1902604.

[9] G. Saravanakumar, H. Park, J. Kim, D. Park, S. Pramanick, D.H. Kim, W.J. Kim, Miktoarm amphiphilic block copolymer with singlet oxygen-labile stereospecific beta-aminoacrylate junction: synthesis, self-assembly, and photodynamically triggered drug release, Biomacromolecules 19 (2018) 2202–2213.

[10] C.Y. Zhao, L.H. Shao, J.Q. Lu, X.W. Deng, Y. Wu, Tumor acidity-induced sheddable polyethylenimine-poly(trimethylene carbonate)/DNA/polyethylene glycol-2,3-dimethylmaleicanhydride ternary complex for efficient and safe gene delivery, ACS Appl. Mater. Interfaces 8 (2016) 6400–6410.

[11] Y. Fang, J.X. Xue, S. Gao, A.Q. Lu, D.J. Yang, H. Jiang, Y. He, K. Shi, Cleavable PEGylation: a strategy for overcoming the "PEG dilemma" in efficient drug delivery, Drug Deliv. 24 (2017) 22–32.

[12] Z.Y. Jiang, J.J. Chen, L.G. Cui, X.L. Zhuang, J.X. Ding, X.S. Chen, Advances in stimuli-responsive polypeptide nanogels, Small Methods 2 (2018) 1700307.

[13] C.Y. Sun, S. Shen, C.F. Xu, H.J. Li, Y. Liu, Z.T. Cao, X.Z. Yang, J.X. Xia, J. Wang, Tumor acidity-sensitive polymeric vector for active targeted siRNA delivery, J. Am. Chem. Soc. 137 (2015) 15217–15224.

[14] V.H. Trang, X.Q. Zhang, R.C. Yumul, W.P. Zeng, I.J. Stone, S.W. Wo, M. M. Dominguez, J.H. Cochran, J.K. Simmons, M.C. Ryan, R.P. Lyon, P.D. Senter, M. R. Levengood, A coiled-coil masking domain for selective activation of therapeutic antibodies, Nat. Biotechnol. 37 (2019) 761–765.

[15] Q.Y. Chen, L.F. Luo, Y.Y. Xue, J. Han, Y. Liu, Y. Zhang, T. Yin, L.H. Wang, D. M. Cun, J.X. Gou, H.B. He, X. Tang, Cisplatin-loaded polymeric complex micelles with a modulated drug/copolymer ratio for improved in vivo performance, Acta Biomater. 92 (2019) 205–218.

[16] X. Yang, Y.J. Yu, X. Huang, Q.X. Chen, H. Wu, R. Wang, R.G. Qi, Y.F. Miao, Y. M. Qiu, Delivery of platinum (II) drugs with bulky ligands in trans-geometry for overcoming cisplatin drug resistance, Mat. Sci. Eng. C-Mater. 96 (2019) 96–104.

[17] X. Feng, W. Xu, J. Liu, D. Li, X. Chen, Polypeptide nanoformulation-induced immunogenic cell death and remission of immunosuppression for enhanced chemoimmunotherapy, Sci. Bull. (2020), https://doi.org/10.1016/j.scib.2020.07.013.

[18] H.Y. Yu, Z.H. Tang, D.W. Zhang, W.T. Song, Y. Zhanga, Y. Yang, Z. Ahmad, X. S. Chen, Pharmacokinetics, biodistribution and in vivo efficacy of cisplatin loaded poly(L-glutamic acid)-g-methoxy poly(ethylene glycol) complex nanoparticles for tumor therapy, J. Contr. Release 205 (2015) 89–97.

[19] J.J. Chen, J.X. Ding, Y.C. Wang, J.J. Cheng, S.X. Ji, X.L. Zhuang, X.S. Chen, Sequentially responsive shell-stacked nanoparticles for deep penetration into solid tumors, Adv. Mater. 29 (2017) 1701170.

[20] Y. Zhang, M.R. Huo, J.P. Zhou, S.F. Xie, PKSolver: an add-in program for pharmacokinetic and pharmacodynamic data analysis in Microsoft Excel, Comput. Meth. Prog. Bio. 99 (2010) 306–314.

[21] Y.Y. Yang, Y.J. Yu, H. Chen, X.X. Meng, W. Ma, M. Yu, Z.Y. Li, C.H. Li, H.L. Liu, X. D. Zhang, H.H. Xiao, Z.Q. Yu, Illuminating platinum transportation while maximizing therapeutic efficacy by gold nanoclusters via simultaneous near-infrared-I/II imaging and glutathione scavenging, ACS Nano 14 (2020) 13536–13547.

[22] Z.Y. Jiang, X.R. Feng, W.G. Xu, X.L. Zhuang, J.X. Ding, X.S. Cheng, Calcium phosphate-cured nanocluster of poly(L-glutamic acid)-cisplatin and arsenic trioxide for synergistic chemotherapy of peritoneal metastasis of ovarian cancer, Acta Polym. Sin. 51 (2020) 901–910.

[23] Y. Liu, D. Li, J. Ding, X. Chen, Controlled synthesis of polypeptides, Chin. Chem. Lett. 31 (2020) 3001–3014.

[24] H.Y. Yu, Z.H. Tang, M.Q. Li, W.T. Song, D.W. Zhang, Y. Zhang, Y. Yang, H. Sun, M. X. Deng, X.S. Chen, Cisplatin loaded poly(L-glutamic acid)-g-methoxy poly (ethylene glycol) complex nanoparticles for potential cancer therapy: preparation, in vitro and in vivo evaluation, J. Biomed. Nanotechnol. 12 (2016) 69–78.

[25] N. Nishiyama, K. Kataoka, Current state, achievements, and future prospects of polymeric micelles as nanocarriers for drug and gene delivery, Pharmacol. Therapeut. 112 (2006) 630–648.

[26] J.B. Gao, F. Wang, S.H. Wang, L. Liu, K. Liu, Y.C. Ye, Z. Wang, H. Wang, B. Chen, J. M. Jiang, J.F. Ou, J.C.M. van Hest, F. Peng, Y.F. Tu, Hyperthermia-triggered on-demand biomimetic nanocarriers for synergetic photothermal and chemotherapy, Adv. Sci. 7 (2020) 1903642.

[27] P. Zheng, Y. Liu, J.J. Chen, W.G. Xu, G. Li, J.X. Ding, Targeted pH-responsive polyion complex micelle for controlled intracellular drug delivery, Chin. Chem. Lett. 31 (2020) 1178–1182.

[28] Z.G. Ren, S.C. Sun, R.R. Sun, G.Y. Cui, L.J. Hong, B.C. Rao, A. Li, Z.J. Yu, Q.C. Kan, Z.W. Mao, A metal-polyphenol-coordinated nanomedicine for synergistic cascade cancer chemotherapy and chemodynamic therapy, Adv. Mater. 32 (2020) 1906024.

[29] C.N. Xu, Y.B. Wang, Z.P. Guo, J. Chen, L. Lin, J.Y. Wu, H.Y. Tian, X.S. Chen, Pulmonary delivery by exploiting doxorubicin and cisplatin co-loaded nanoparticles for metastatic lung cancer therapy, J. Contr. Release 295 (2019) 153–163.

[30] P.S. Kulkarni, M.K. Haldar, R.R. Nahire, P. Katti, A.H. Ambre, W.W. Muhonen, J. B. Shabb, S.K.R. Padi, R.K. Singh, P.P. Borowicz, D.K. Shrivastava, K.S. Katti, K. Reindl, B. Guo, S. Mallik, MMP-9 responsive PEG cleavable nanovesicles for efficient delivery of chemotherapeutics to pancreatic cancer, Mol. Pharm. 11 (2014) 2390–2399.

[31] C. Huang, Y. Sun, M. Shen, X.Y. Zhang, P. Gao, Y.R. Duan, Altered cell cycle arrest by multifunctional drug-loaded enzymatically-triggered nanoparticles, ACS Appl. Mater. Interfaces 8 (2016) 1360–1370.

[32] J. Aujard-Catot, M. Nguyen, C. Bijani, G. Pratviel, C. Bonduelle, Cd^{2+} coordination: an efficient structuring switch for polypeptide polymers, Polym. Chem. 9 (2018).

[33] C. Bonduelle, F. Makni, L. Severac, E. Piedra-Arroni, C.L. Serpentini, S. Lecommandoux, G. Pratviel, Smart metallopoly(L-glutamic acid) polymers: reversible helix-to-coil transition at neutral pH, RSC Adv. 6 (2016) 84694–84697.

[34] C. Zhang, J.H. Lu, F.L. Tian, L.D. Li, Y.Q. Hou, Y.Y. Wang, L.D. Sun, X.H. Shi, H. Lu, Regulation of the cellular uptake of nanoparticles by the orientation of helical polypeptides, Nano Res 12 (2019) 889–896.

[35] J. Chen, Z. Jiang, W. Xu, T. Sun, X. Zhuang, J. Ding, X. Chen, Spatiotemporally targeted nanomedicine overcomes hypoxia-induced drug resistance of tumor cells after disrupting neovasculature, Nano Lett. 20 (2020) 6191––6198.

[36] M. Shariati, G. Lollo, K. Matha, B. Descamps, C. Vanhove, L. Van de Sande, W. Willaert, L. Balcaen, F. Vanhaecke, J.P. Benoit, W. Ceelen, S.C. De Smedt, K. Remaut, Synergy between intraperitoneal aerosolization (PIPAC) and cancer nanomedicine: cisplatin-loaded polyarginine-hyaluronic acid nanocarriers efficiently eradicate peritoneal metastasis of advanced human ovarian cancer, ACS Appl. Mater. Interfaces 12 (2020) 29024–29036.

[37] R.G. Qi, Y.H. Wang, P.M. Bruno, H.H. Xiao, Y.J. Yu, T. Li, S. Lauffer, W. Wei, Q. X. Chen, X. Kang, H.Q. Song, X. Yang, X. Huang, A. Detappe, U. Matulonis, D. Pepin, M.T. Hemann, M.J. Birrer, P.P. Ghoroghchian, Nanoparticle conjugates of a highly potent toxin enhance safety and circumvent platinum resistance in ovarian cancer, Nat. Commun. 8 (2017) 2166.